Dual-parameter sensing based on symmetrically chirped long-period fiber grating*

HUANG Qiuping[1], ZHU Xiaoshuai[1], REN Ziyan[1], CHEN Haiyun[1, 2, *], LING Qiang[3], PENG Baojin[1, 2], CHEN Daru[3]

1. College of Physics and Electronic Information Engineering, Zhejiang Normal University, Jinhua 321004, China
2. Institute of Information Optics, Zhejiang Normal University, Jinhua 321004, China
3. Hangzhou Institute of Advanced Studies, Zhejiang Normal University, Hangzhou 311231, China

Abstract

A dual-parameter sensor based on a symmetrically chirped long-period fiber grating (SCLPFG) is proposed and demonstrated. The SCLPFG consists of two segments of long-period fiber gratings (LPFGs) with the same length and average period but opposite chirp coefficients, forming an in-fiber Mach-Zehnder interferometer (MZI). Due to the chirping effect of the LPFG, the core mode at different wavelength couples to the cladding modes at different positions within the positively chirped LPFG. Integrated with the symmetry of the SCLPFG, the stimulated cladding mode recouples to the core at the symmetrical position in the negatively chirped LPFG. Consequently, in this MZI configuration, the effective length of the interference arm is not fixed but varies with wavelength. As a result, the transmission spectrum of the SCLPFG is characterized by a nonuniform fringe pattern where the free spectrum range (FSR) increases with wavelength increasing. For the MZI-based fiber sensor, the phase difference between the core and cladding modes, influenced by environmental parameters, plays a crucial role in determining sensitivity, as this phase difference is directly proportional to the length of the interference arm. Therefore, for a specific measurand, the sensitivities interrogated by the dips at different wavelengths in the fringe pattern are inherently different, which leads to the possibility of multi-parameter sensing through a differential modulation method.The fringe characteristics and sensing mechanism are systematically investigated through theoretical analysis and numerical simulation. In the

* The paper is an English translated version of the original Chinese paper published in Acta Physica Sinica. Please cite the paper as: HUANG Qiuping, ZHU Xiaoshuai, REN Ziyan, CHEN Haiyun, LING Qiang, PENG Baojin, CHEN Daru，**Dual-parameter sensing based on symmetrically chirped long-period fiber grating**. *Acta Phys. Sin.*, 2025, 74(16): 164211. doi: 10.7498/aps.74.20250449

experimental section, the SCLPFG structure is engraved on a Corning single-mode fiber by irradiating photosensitive core with point-by-point UV pulsed laser. The grating exhibits an average period of 321 μm and a chirping coefficient of ±21.9 μm/cm, with the total length of the symmetrically chirped grating determined to be 4.34 cm. Experimental implementation of simultaneous dual-parameter sensing for surrounding refractive index (SRI) and temperature is conducted, verifying the differential response of distinct fringe dips to SRI and temperature variations. A 2×2 sensitivity coefficient matrix is established by linearly fitting the SRI and temperature response data, which are obtained by interrogating two dips at different wavelengths. Thus, the variations of SRI and temperature are determined by multiplying the inverse sensitivity coefficient matrix with the wavelength shift array. Furthermore, temperature sensitivities are corrected by considering the thermal effect on the refractive index of the liquid. Finally, the maximum sensitivity of the sensor to SRI is –95.316 nm/RIU and a maximum sensitivity to temperature is 0.0849 nm/℃, both of which have excellent linearity. This sensing scheme features a compact structure, high sensitivity, and the ability to measure multiple parameters. Moreover, the multi-channel nonuniform fringe characteristics enable the sensor configuration to be extended for simultaneous measurement of three or more parameters, thus providing a promising lab-on-fiber platform for multi-parameter sensing applications.

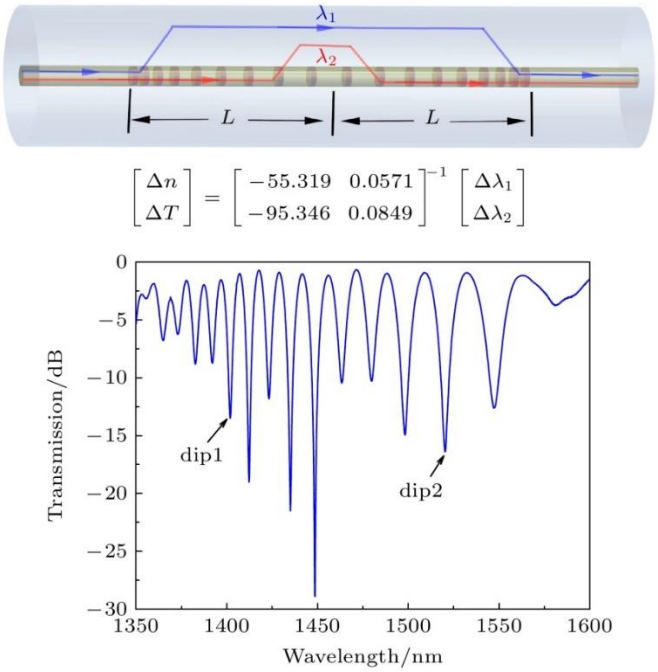

Keywords: symmetrically chirped long-period fiber grating; dual-parameter sensing; refractive index; temperature

PACS: 42.81.–i; 07.07.Df; 42.25.Hz

doi: 10.7498/aps.74.20250449

cstr: 32037.14.aps.74.20250449

1. Introduction

In recent years, fiber-optic sensor has been paid more and more attention due to its high sensitivity, strong anti-electromagnetic interference ability, good network compatibility and other advantages, and has been widely used in the measurement of environmental parameters such as refractive index[1–3], temperature[4–6], humidity[7,8], pressure[9,10], gas concentration[11,12] and solution ion concentration[13,14]. High sensitivity is the prominant advantage of optical fiber sensor, but the structure and material properties of optical fiber are affected by temperature, so the crosstalk of multiple parameters is an unavoidable problem in optical fiber sensing technology. Therefore, solving the crosstalk between different parameters and realizing the simultaneous measurement of multiple parameters is an important research direction of optical fiber sensor[15–21].

At present, the optical fiber multi-parameter sensing mechanism is mainly realized[15–17] by combining optical fiber structures with different sensing characteristics, but the excellent characteristics of the original single sensor are often difficult to be guaranteed at the same time in this composite structure, which leads to incompatibility, instability, reduced sensitivity and mechanical strength, and crosstalk, thus affecting the overall performance of the multi-parameter sensor. Multi-parameter sensing based on a single fiber structure has also been reported. As early as 1997, Bhatia et al.[18] proposed a dual-parameter sensing method based on a single long-period fiber grating (LPFG), which utilizes the differential response of resonance peaks corresponding to different cladding mode coupling in LPFG to achieve simultaneous measurement of stress and temperature through differential matrix demodulation, but the sensitivity is low. Since then, multi-parameter sensors based on LPFG have emerged endlessly, and their sensing performance has been continuously optimized. Ling et al. [19] used CO_2 laser to inscribe LPFG in few-mode fiber, and realized the simultaneous measurement of surrounding refractive index (SRI) and temperature by using the difference of coupling between cladding mode and core mode of LP_{01} and LP_{11}. Zhao et al.[20] used a CO_2 laser to write LPFG on a few-mode ring-core fiber by single-side illumination, and used asymmetric coupling characteristics to achieve simultaneous measurement of vector bending, torsion and temperature. Zhang et al.[21] designed a LPFG structure composed of polarization-maintaining fiber and single-mode fiber, and realized the simultaneous measurement of bending and torsion through polarization multiplexing. Esposito et al.[22] fabricated LPFG in polarization-maintaining panda fiber by arc discharge method, and investigated the changes of three resonance peaks produced by different cladding mode coupling, and realized the simultaneous measurement of temperature, stress and torsion combined with polarization characteristics. Urrutia et al.[23] used ultraviolet point-by-point exposure method to fabricate LPFG, and coated PAH/PAA film on the grating cladding, and used different resonance peaks generated by LPFG in coated/uncoated areas to measure humidity and temperature simultaneously. In order to meet the differential response requirements of multi-parameter sensing,

the above single-grating structure usually requires the use of special structure fibers, or requires additional coating, which is relatively complex and costly. Liu et al.[24] used femtosecond laser to inscribe a single phase-shifted LPFG working near the phase matching turning point in a common single-mode fiber. The π phase shift and double-peak resonance effect produce four different loss peaks in the transmission spectrum. Through matrix demodulation, the four parameters of temperature, stress, refractive index and pH can be measured simultaneously. However, it is not easy to accurately inscribe the LPFG working near the phase matching turning point in a limited wavelength range. The process parameters need to be adjusted through iterative experimentation, and the process is complex.

In this paper, a compact multi-parameter sensor structure based on a symmetrically chirped long-period fiber grating (SCLPFG) is proposed, which is fabricated in a single-mode fiber by conventional UV point-by-point exposure method. The symmetrical chirped LPFG is composed of two successive linear chirped sub-gratings with opposite chirp coefficients and the same average period and length. The chirp effect makes the fiber core modes with different wavelengths coupled to the cladding mode at different positions by the first sub-grating, and the symmetrical chirp structure makes the cladding mode re-coupled back to the fiber core at the symmetrical position of the second sub-grating, so the equivalent interference arm lengths corresponding to different wavelengths are different, thus forming Mach-Zehnder interference with gradually changing interference arm lengths. Therefore, the transmission spectrum of the symmetrically chirped LPFG is characterized by nonuniform MZI interference fringes with gradually changing spatial frequencies, and the interference dips at different wavelength positions have different response characteristics to the same parameter, so that simultaneous measurement of multiple parameters can be realized by matrix demodulation. In this paper, the interference mechanism and spectral characteristics of symmetrically chirped LPFG are systematically analyzed, and the multi-parameter sensing application of symmetrically chirped LPFG is demonstrated by taking the two parameters of SRI and temperature as an example, which provides a new technical idea for the development of optical fiber multi-parameter sensing technology.

2. Theoretical analysis

The structure of the symmetrically chirped long-period fiber grating is shown as Fig. 1, the grating period Λ increases first and then decreases along the axial direction of the fiber to form a symmetrical structure. Two sub-gratings with opposite chirp coefficients and the same average period and length are arranged on both sides of the center point. The period of a single linearly chirped sub-grating can be expressed as[8]

$$\Lambda(z) = \Lambda_0 + C(z - L/2), \quad (1)$$

where, z is the axial coordinate along the fiber, and the origin is located at the left edge of the sub-grating; Λ_0 is the average period of the sub-grating, that is, the period of the midpoint position of the sub-grating; and C is the chirp coefficient. In the symmetrical grating structure shown in Fig. 1, C of the left sub-grating is positive, while that of the right sub-grating is negative.

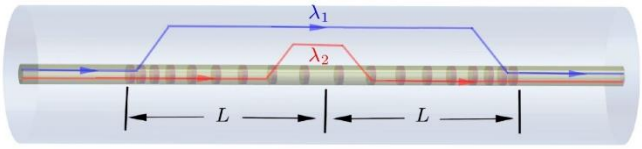

Figure 1. Schematic diagram of symmetrically chirped LPFG.

According to the coupled-mode theory of long-period fiber gratings, the resonant wavelength of chirped LPFG is determined by the phase-matching condition[25]:

$$\lambda_{\text{res}}(z) = (n_{\text{eff}}^{\text{co}} - n_{\text{eff}}^{\text{cl},m})\Lambda(z), \quad (2)$$

where $n_{\text{eff}}^{\text{co}}$ and $n_{\text{eff}}^{\text{cl},m}$ are the effective refractive indices of the core mode and mth cladding mode, respectively. It can be seen from Eq. (2) that the resonant wavelength of the chirped LPFG is related to the position z. The core mode with different wavelength is coupled to the cladding modes at different positions of the left sub-grating, and the cladding modes are re-coupled back to the core at the symmetrical positions of the right sub-grating, forming a Mach-Zehnder interference effect[26] with the core mode:

$$I = I_{\text{co}} + \alpha I_{\text{cl}}^{m} - 2\sqrt{\alpha I_{\text{co}} I_{\text{cl}}^{m}}\cos\,\theta, \quad (3)$$

where I_{co} and I_{cl}^{m} are the intensities of the core and mth cladding modes, respectively; α is the attenuation coefficient of the cladding mode; and θ is the phase difference:

$$\theta = \frac{2\pi}{\lambda}(n_{\text{eff}}^{\text{co}} - n_{\text{eff}}^{\text{cl},m})L_{\text{p}}, \quad (4)$$

In Eq. (4), L_{p} is the distance between the *coupling* position of light with different wavelengths from the left grating to the *re-coupling* position of the right grating, that is, the interference arm length in the MZI. The symmetrical chirp structure and coupling characteristics of the SCLPFG determine that L_{p} is not a constant value. It can be obtained from Eq. (1) and the structure shown in Fig. 1 that

$$L_{\text{p}} = L - \frac{2}{C}[\Lambda(z) - \Lambda_0], \quad (5)$$

which implies that L_p decreases with the increase of grating period. Since the grating resonant wavelength increases with the grating period, as regulated by Eq. (2), L_p decreases with the increase of wavelength. In the interference fringes, when the phase difference in Eq. (4) is an odd multiple of π, the interference minimum is reached at a specific wavelength, that is, the wavelength position of the interference dip:

$$\lambda_k = \frac{2\Delta n_{\text{eff}} L_p}{2k+1}, \tag{6}$$

where k = 0, 1, 2, ⋯; $\Delta n_{\text{eff}} = n_{\text{eff}}^{\text{co}} - n_{\text{eff}}^{\text{cl},m}$, and the wavelength interval between two adjacent interference dips is

$$\Delta\lambda \approx \frac{\lambda^2}{\Delta n_{\text{eff}} L_p}, \tag{7}$$

where $\Delta\lambda$ represents the free spectral range (FSR). It can be seen from Eq. (7) that the interference fringe FSR produced by the SCLPFG structure is not only affected by the wavelength itself, but also related to L_p. Combined with Eq. (5), it can be seen that the fringe FSR increases significantly with the wavelength, that is, the spatial frequency decreases with the wavelength. At the same time, it can be seen from Eq. (6) that for the same environmental parameter (such as refractive index n or temperature) change, the dip wavelength offset at different wavelengths will be significantly different due to varying L_p. This differential response characteristic lays the foundation for multi-parameter sensing based on differential matrix demodulation.

According to the coupled mode theory, the transmission spectrum of SCLPFG can be simulated by the transfer matrix method. The whole grating structure is divided into multiple segments, and each segment is approximately regarded as a uniform LPFG. The transmission of light through a single uniform LPFG can be expressed by a matrix[25]:

$$\boldsymbol{M} = \begin{bmatrix} \cos(\gamma_j L_j) + \mathrm{i}\frac{\overline{\sigma_j}}{\gamma_j}\sin(\gamma_j L_j) & \mathrm{i}\frac{\kappa}{\gamma_j}\sin(\gamma_j L_j) \\ \mathrm{i}\frac{\kappa}{\gamma_j}\sin(\gamma_j L_j) & \cos(\gamma_j L_j) - \mathrm{i}\frac{\overline{\sigma_j}}{\gamma_j}\sin(\gamma_j L_j) \end{bmatrix}, \tag{8}$$

where i is the imaginary unit; L_j is the length of the jth grating segment; $\gamma_j^2 = \overline{\sigma}_j^2 + \kappa\kappa^*$,$\kappa$ is the coupling coefficient between the core mode and the cladding mode, $\overline{\sigma}_j = \delta_j + \kappa_{\text{co}}/\underline{\kappa_{\text{co}}}22$, where κ_{co} is the self-coupling coefficient of the core mode, and δ_j is the detuning parameter:

$$\delta_j = \frac{\pi}{\lambda}(n_{\text{eff}}^{\text{co}} - n_{\text{eff}}^{\text{cl},m}) - \frac{\pi}{\Lambda_j}, \tag{9}$$

where Λ_j is the period of the jth grating segment.

The simulated transmission fringe of SCLPFG is shown in Fig. 2, where the parameters in simulation are Λ_0 = 321 μm, L = 2.1 cm, C = ±22 μm/cm. The transmission spectrum is characterized as high-contrast nonuniform interference fringes where the FSR increases with wavelength. For example, FSR_1 and FSR_2 at short and long wavelengths marked in Fig. 2 are 11. 4 nm and 27. 6 nm, respectively. It should be pointed out that if the grating period in Fig. 1 decreases first and then increases along the axial direction, a symmetrically chirped LPFG structure can also be formed, but the variation trend of the fringe frequency is opposite to that shown in the Fig. 2, the fringe frequency on the short wavelength side is low, while the fringe frequency on the long wavelength side is high.

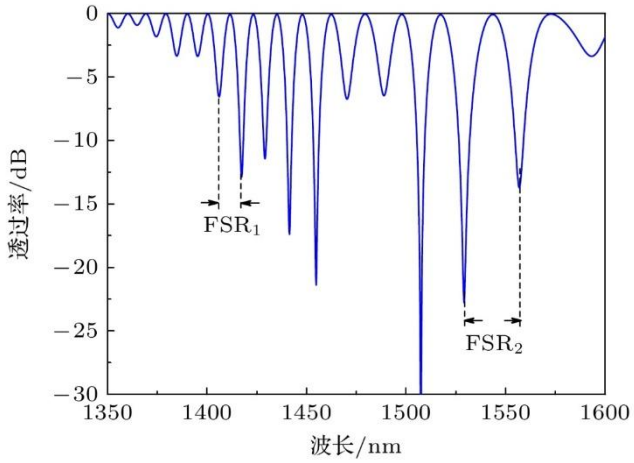

Figure 2. Simulated transmission spectrum of symmetrically chirped LPFG.

The nonuniform fringe characteristics of the symmetrical chirped LPFG can be deeply analyzed by Fourier transform. The Fourier spectrum of the fringes in Fig. 2 is illustrated by the red solid line in Fig. 3(a), and the characteristic peaks of the broad spectrum are presented in the spectrum. For comparison, the Fourier spectrum of the cascaded chirped LPFG is also given in Fig. 3(a). The cascaded chirped LPFG[8] is formed by directly cascading two chirped LPFGs with the same chirp coefficients, that is, the grating on the right side is exactly the same as the grating on the left side in Fig. 1. At this time, the interference arm length corresponding to different wavelengths is a constant L, and the interference fringes are nearly uniform except for a slight change in the FSR related to the wavelength, as shown by the blue dotted line in Fig. 3(b). A comparison tells that the characteristic spectrum of SCLPFG is regarded as the broadened characteristic spectrum of the cascaded chirped LPFG with reduced peak value, which means that the fringes of SCLPFG contain more frequency components and the spectrum range is wider. This is because the symmetrical chirped structure makes the length of the interference arm of the MZI no longer a fixed value L, but varies with the wavelength, resulting in a significant increase in the frequency component of the fringe. Fig. 3(b) and Fig. 3(c) show the recovered phase curves after filtering the characteristic spectra of the two grating structures, and display them synchronously with the

original fringe signals. It can be seen from Fig. 3(b) that the phase of the cascaded chirped LPFG increases approximately linearly with wavelength, and the corresponding transmittance exhibits a cosine modulation with wavelength with equal period, that is, the fringe FSR is nearly uniform. However, the phase of the SCLPFG shown in Fig. 3(c) exhibits an obvious curve trend with wavelength, and the slope of the phase curve decreases with wavelength. Therefore, the corresponding fringe frequency decreases with wavelength, showing a non-uniform fringe feature with increasing FSR, which is consistent with the theoretical analysis.

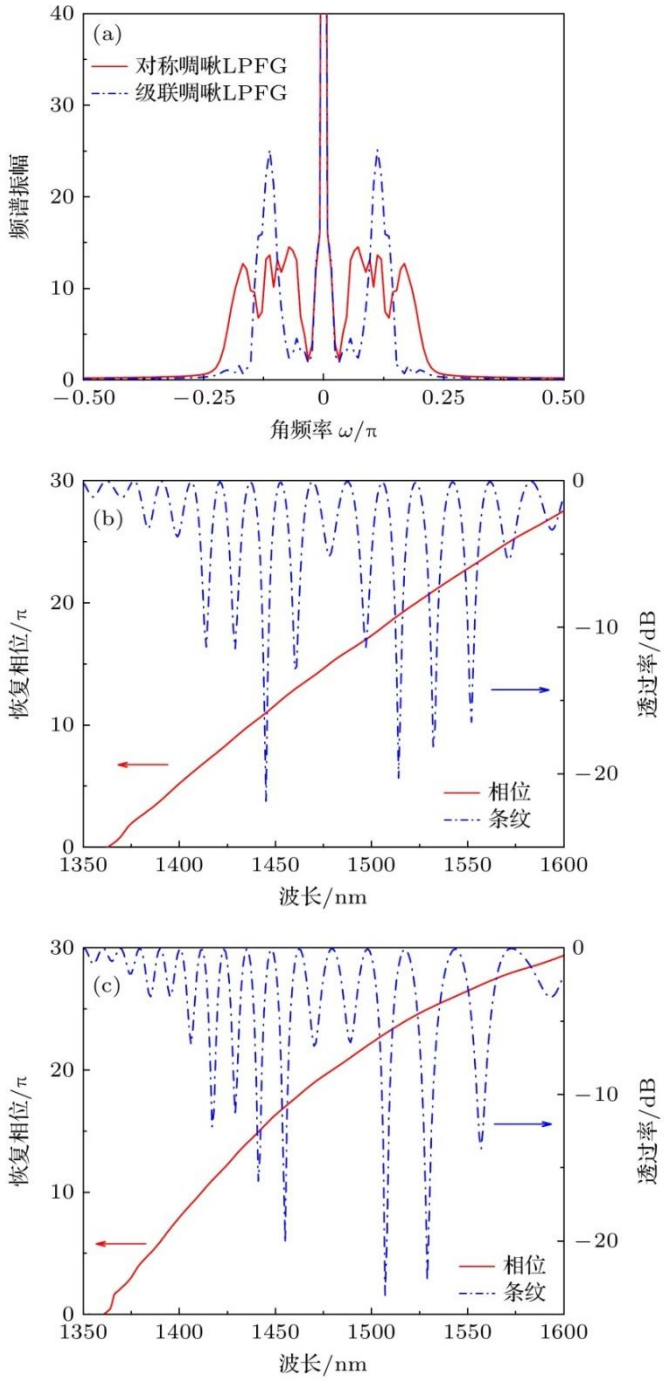

Figure 3. Fourier analysis for the fringe: (a) Frequency spectrum; (b) recovered phase of cascaded chirped LPFG; (c) recovered phase of symmetrically chirped LPFG.

3. Experimental results and analysis

Symmetrically chirped long-period fiber gratings were written into a single-mode fiber (Corning SMF-28) by UV point-by-point exposure. The single-mode fiber was loaded with hydrogen at 120 ATM (1 ATM = 101325 Pa) for a week to improve the photosensitivity of the Ge-doped core. The light source was a 213 nm ultraviolet pulsed laser with a pulse power of 137 mW, a frequency of 12 kHz, a spot diameter of 80 μm, and a single exposure time of 10 s. The period of the grating on the left side is increased from 296 μm to 343 μm with a step size of 3 μm, and each period value is inscribed with 4 periods. The grating on the left side has a length *L* of 2.17 cm and an equivalent chirp coefficient of 21.9 μm/cm, while the grating on the right side is symmetrically inscribed in the same way, with a period reduced from 343 μm to 296 μm and an equivalent chirp coefficient of – 21.9 μm/cm. The fabricated grating was annealed at 120 ℃ for 12 hours to enhance the spectral stability.

The transmission spectrum of SCLPFG in the experiment is shown by the red solid line in Fig. 4(a), and the fringe FSR increases gradually with the wavelength, which is basically consistent with the numerical simulation fringe spectrum under the same parameters. Fig. 4(b) shows the transmission fringe spectrum in air and in water. Similar to the general LPFG sensing, the increase of the surrounding refractive index makes the spectrum blue shift. However, the interference dip wavelength offsets of different FSRs are significantly different. The marked *dip1* and *dip2* in the figure shift by 4.6 nm and 7.2 nm respectively, which reflects the difference of the response to the change of the same environmental parameter and lays a foundation for the construction of multi-parameter sensors. The response to SRI and temperature will be characterized by the wavelength shift of dip1 and dip2 in the subsequent sensing test.

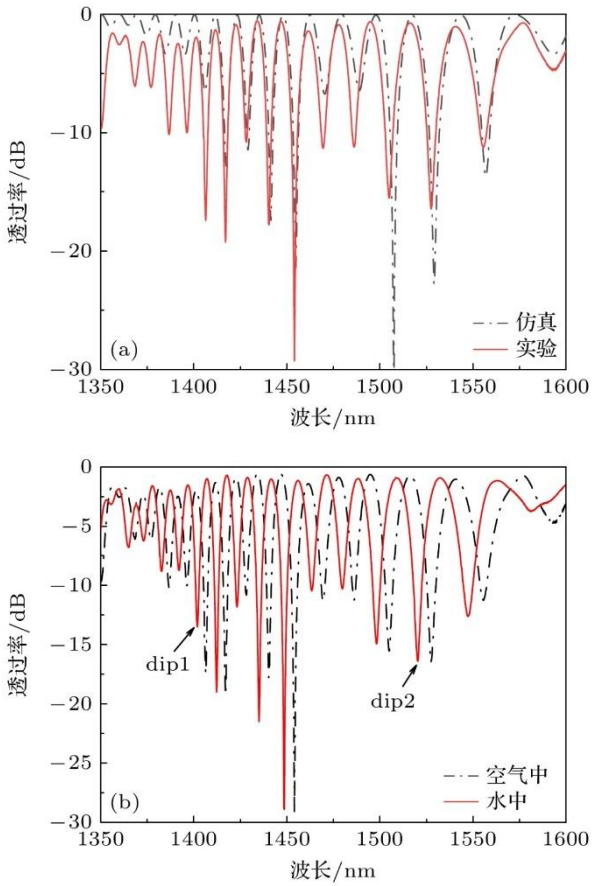

Figure 4. Transmission spectrum of SCLPFG: (a) Comparison between the experimental and simulated spectra; (b) comparison between the spectra in air and water.

The experimental device for surrounding refractive index and temperature response test is shown in Fig. 5. The sensor is placed in a metal container and fixed in a straight state to avoid the influence of bending. The light emitted by the broadband light source passes through the sensor and is received and displayed by a spectrometer (Anristu, MS9740A). The metal container is placed on a heating platform. Glycerin solutions with mass concentrations ranging from 0% to 40% were used to simulate different surrounding refractive indices[19]. The temperature was kept at 20 ℃ during the SRI response test.

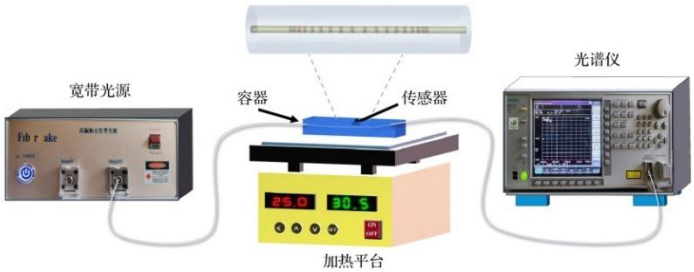

Figure 5. Schematic diagram of the setup for SRI and temperature measurements.

The change of fringe pattern under different SRI is shown in the inset of Fig. 6. Both dip1 and dip2 show blue shift with the increase of SRI. The overall blue shift characteristic is the same as

the known response characteristic of LPFG to SRI, but the offset of dip2 is much larger than that of dip1. The data with error bars obtained from five repeated measurements of refractive index are given in Fig. 6. The linear fitting results show that within the SRI range of 1.3333-1.3841 the response sensitivities of dip1 and dip2 to SRI are – 55.319 nm/RIU and – 95.346 nm/RIU, respectively, the standard errors of the linear fitting slopes are ± 2.496 and ± 4.999, respectively, and R^2 are 0.981 and 0.975, respectively.

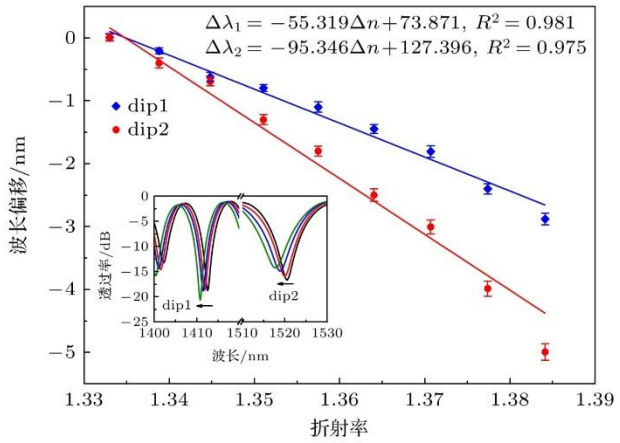

Figure 6. Sensing characteristics to SRI variation.

During the temperature response test, the container is filled with pure deionized water, which is heated by the heating platform. The spectrum is recorded every 6 ℃ in the range of 12-80 ℃, and the spectral data of 12 temperature points are recorded. The temperature is kept stable for more than 5 minutes during the measurement of each temperature value. As shown in the inset of Fig. 7, the fringe pattern shifts to longer wavelengths with increasing temperature, and dip2 also has a larger offset relative to dip1. The data with error bars obtained from five repeated temperature measurements are also given in the Fig. 7. The linear fitting results show that the response sensitivity of dip1 and dip2 to temperature is 0.0627 nm/℃ and 0.0859 nm/℃, respectively, the standard error of the linear fitting slope is ± 0.0008 and ± 0.0012, respectively, and both R^2 are 0.998, showing good linearity.

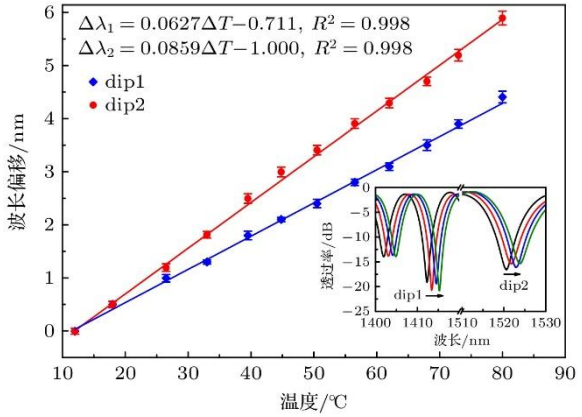

Figure 7. Sensing characteristics to temperature variation.

The experimental results of SRI and temperature detection verify the differential response characteristics of dip1 and dip2 in the interference fringe patterns of SCLPFG to the same environmental parameters. For the dual-parameter sensing of SRI and temperature, the wavelength shifts $\Delta\lambda_1$ and $\Delta\lambda_2$ of dip1 and dip2 are related to the variations Δn, ΔT of SRI and temperature as follows:

$$\begin{bmatrix}\Delta\lambda_1\\ \Delta\lambda_2\end{bmatrix} = \begin{bmatrix}K_{n1} & K_{T1}\\ K_{n2} & K_{T2}\end{bmatrix}\begin{bmatrix}\Delta n\\ \Delta T\end{bmatrix}, \quad (10)$$

where K_{n1} and K_{n2} are the response sensitivity coefficients of dip1 and dip2 to SRI; K_{T1} and K_{T2} are the response sensitivity coefficients of dip1 and dip2 to temperature. When measuring the unknown SRI and temperature, the variation of SRI and temperature can be calculated by the corresponding matrix:

$$\begin{bmatrix}\Delta n\\ \Delta T\end{bmatrix} = \begin{bmatrix}K_{n1} & K_{T1}\\ K_{n2} & K_{T2}\end{bmatrix}^{-1}\begin{bmatrix}\Delta\lambda_1\\ \Delta\lambda_2\end{bmatrix}. \quad (11)$$

It should be pointed out that the refractive index of liquid decreases with the increase of temperature, so the fringe movement caused by the change of liquid temperature is actually the result of the direct change of temperature and the indirect change of liquid refractive index. Assuming that the sensor response to SRI variation is independent of temperature, the experimentally measured temperature sensitivity can be expressed as[27]

$$K_{Tj} = \hat{K}_{Tj} + K_{nj}R_{n,T}(j = 1,2), \quad (12)$$

where, $\hat{K}_{Tj}$ is the sensitivity of the sensor when it is affected by temperature alone; The K_{nj} is the SRI response sensitivity at 20 ℃, and the $R_{n,T}$ is the temperature coefficient of the liquid. For the water used as the solvent in the experiment, the temperature coefficient is $R_{n,T} = 1.02 \times 10^{-4}$[27], so the temperature sensitivity K_{Tj} in Eq. (11) should be corrected as $\hat{K}_{Tj}$. According to Eq. (12) and the fitting results of Fig. 6 and Fig. 7, the sensitivity of dip1 and dip2 in the fringe to temperature can be calculated, which is 57.1 pm/℃ and 84.9 pm/℃, respectively. Therefore, Eq. (11) can be expressed explicitly as

$$\begin{bmatrix}\Delta n\\ \Delta T\end{bmatrix} = \begin{bmatrix}-55.319 & 0.0571\\ -95.346 & 0.0849\end{bmatrix}^{-1}\begin{bmatrix}\Delta\lambda_1\\ \Delta\lambda_2\end{bmatrix}. \quad (13)$$

When the temperature and the refractive index of the liquid change at the same time, the change of the temperature and the SRI can be calculated by measuring the wavelength offset of dip1 and

dip2 and substituting in Eq. (13). It should be noted that the above theoretical analysis and experimental test only take the simultaneous measurement of temperature and SRI as an example to conceptually verify and demonstrate the multi-parameter sensing capability of SCLPFG. Since the interference fringes of SCLPFG contain multiple interference dips with different FSRs, in principle, the proposed sensor can be extended to the simultaneous measurement of three or more parameters. In addition, the refractive index sensitivities – 55.319 nm/RIU and – 95.346 nm/RIU of the sensor are measured in the low SRI range of 1.3333 — 1.3841, and a higher sensitivity[1] can be achieved in the SRI range close to the refractive index of the cladding, and it can also be improved by means of etching the cladding[27], depositing a high refractive index nano-film[23,26], designing the grating operating near the dispersion turning point[2,24], or using a special optical fiber[19–22].

4. Conclusion

In this paper, a dual-parameter sensor based on a symmetrically chirped long-period fiber grating is proposed and demonstrated. The symmetrically chirped grating structure makes the transmission spectrum show a non-uniform fringe structure with gradually changing frequency. The wavelength shift of the interference dip at different wavelength positions has significantly different response sensitivity to the change of the same environmental parameter, which makes SCLPFG have multi-parameter sensing ability. The fringe spectral characteristics of SCLPFG are analyzed theoretically and numerically. The symmetrically chirped LPFG structure is fabricated by UV point-by-point exposure method, and the dual-parameter sensing ability of symmetrically chirped LPFG is verified by the detection of SRI and temperature. The response sensitivities of SRI and temperature are – 95.316 nm/RIU and 0.0849 nm/℃, respectively. It should be specially pointed out that the interference arm length of MZI in SCLPFG changes with the wavelength, the differential response to the same parameter is realized by using the special spectral characteristics generated by a single grating structure, and the multi-parameter sensing is realized by matrix demodulation. Different from other multi-parameter sensing technologies based on the combination of multiple fiber structures or the combination of a single grating structure and polarization control, the sensor can be made only by ultraviolet irradiation in a common single-mode fiber, and the structure and principle are simple. More importantly, there are multiple interference dips corresponding to different interference arm lengths at different wavelength positions in the interference fringe pattern of SCLPFG, so it can be extended to the simultaneous measurement of three or more parameters, and has important practical application value in the field of optical fiber sensing based on refractive index response.

References

[1] Gao S, Liu Y, Yang J, Duan Z Y, Yin T A, Liu Z H, Shi J H, Yuan L B, Guan C Y 2024 *J. Lightwave Technol.* **42** 1696

[2] Liu S, Zhou M, Zhang Z, Sun Z Y, Bai Z Y, Wang Y P 2022 *Opt. Lett.* **47** 2602

[3] Hao J Q, Han B C 2020 *Acta Opt. Sin.* **40** 0206002

[4] Tian T, Li M, Ma Y W, Geng T, Yuan L B 2023 *Opt. Lett.* **48** 2785

[5] Wang J B, Hao J Y, Zhou J, Wang A Z, Zeng X Z, Yang X Y, Meng H R, Li S, Yang Q, Sun W M, Geng T 2023 *Sens. Actuators, A* **359** 114465

[6] Yang Y, Xu B, Liu Y M, Li P, Wang D N, Zhao C L 2017 *Acta Phys. Sin.* **66** 094205

[7] Chen P Y, Zhong N B, He X F, Xie Q H, Wan B, He Y Y, Wu L, Liu Y, Lai D 2024 *Acta Opt. Sin.* **44** 0428003

[8] Chen H Y, Gu Z T, Gao K 2014 *Sens. Actuators, B* **196** 18

[9] Ding Y L, Chen Y, Luo S, Ling Q, Zhang Y S, Yu Z W, Guan Z G, Chen D R 2024 *Opt. Laser Technol.* **171** 110414

[10] Chen Y, Luo W X, Jiao B B, Yan Y X, Ling Q, Chen H Y, Yu Z W, Guan Z G, Chen D R 2024 *J. Lightwave Technol.* **42** 463

[11] Yue Y, Hu X X, Zhou R, Wang R H, Qiao X G 2023 *J. Lightwave Technol.* **41** 2578

[12] Zhu X S, Ling Q, Ren Z Y, Chen H Y, Zhou R J, Wang Y, Lou G, Luo S, Yu Z W, Guan Z G, Chen D R 2025 *Opt. Laser Technol.* **182** 112232

[13] Ghosh S, Dissanayake K, Asokan S, Sun T, Rahman B M A, Grattan K T V 2022 *Sens. Actuators, B* **364** 131818

[14] Li X L, Zhao H Y, Wu W J, Jiang W F, Zheng J J, Zhang Z X, Yu K H, Wei W 2022 *Acta Phys. Sin.* **71** 050702

[15] Liu Y G, Yang D Q, Wang Y X, Zhang T, Shao M, Yu D, Fu H W, Jia Z N 2019 *Opt. Commun.* **443** 166

[16] Zhang P, Tang M, Gao F, Zhu B P, Fu S N, Ouyang J, Shum P P, Liu D M 2014 *Opt. Express* **22** 19581

[17] Zhao Y, Zhao J, Wang X X, Peng Y, Hu X G 2022 *Sens. Actuators, B* **353** 131134

[18] Bhatia V, Campbel D, Claur R O 1997 *Opt. Lett.* **22** 648

[19] Ling Q, Gu Z T, Pang B 2020 *Opt. Fiber Technol.* **58** 102264

[20] Zhao Y, Chen S, Guo Y, Jiang Y, Chen S, Mou C, Liu Y, He Z 2024 *Opt. Laser Technol.* **175** 110879

[21] Zhang S, Geng T, Sun W M 2022 *Opt. Lett.* **47** 2266

[22] Esposito F, Srivastava A, Iadicicco A, Campopiano S 2019 *Opt. Laser Technol.*

113 198

[23] Urrutia A, Goicoechea J, Ricchiuti A, Barrera D, Sales S, Arregui F 2016 *Sens. Actuators, B* **227** 135

[24] Liu T, Li Y W, Dai X Y, Gan W B, Wang X S, Dai S X, Song B A, Xu T F Zhang P Q 2023 *J. Lightwave Technol.* **41** 5169

[25] Erdogan T 1997 *J. Lightwave Technol.* **15** 1277

[26] James S W, Ishaq I, Ashwell G J, Tatam R P 2005 *Opt. Lett.* **30** 2197

[27] Yan J H, Zhang A P, Shao L Y, Ding J F, He S L 2007 *IEEE Sens. J.* **7** 1360